Nanoscale Advances

ROYAL SOCIETY OF CHEMISTRY

PAPER

View Article Online
View Journal | View Issue

Cite this: *Nanoscale Adv.*, 2020, **2**, 746

A highly reliable, impervious and sustainable triboelectric nanogenerator as a zero-power consuming active pressure sensor†

Venkateswaran Vivekananthan, [a] Arunkumar Chandrasekhar, [ab] Nagamalleswara Rao Alluri, [a] Yuvasree Purusothaman [a] and Sang-Jae Kim *[a]

The triboelectric effect is one of the most trending effects in energy harvesting technologies, which use one of the most common effects in daily life. Herein, an impervious silicone elastomer-based triboelectric nanogenerator (SE-TENG) is reported with a micro roughness-created silicone elastomer film and Ni foam as triboelectric layers with opposite surface charges. The surface roughness modification process was performed *via* a cost-effective soft lithography technique using sandpaper. The replicated film was then used as the negative triboelectric layer and porous Ni foam was used as the positive triboelectric layer. The device exhibited the advantage of high stability due to the porous nature of the Ni foam, which could not damage the roughness pattern of the elastomer film. The device generated a maximum electrical output of ~370 V/6.1 μA with a maximum area power density of ~17 mW m^{-2} at a load resistance of 1 GΩ. Furthermore, the SE-TENG device was packed using polyethylene to protect it from humidity and made to be a water-resistant SE-TENG (WR-SE-TENG). The device was stable under different percentages of relative humidity, showing a uniform electrical output in the range of 10% RH to 99% RH. This proves that the packing is highly resistant against moisture and humidity. The device was also used for demonstrating its capability in powering small electronic components such as charging commercial capacitors, glowing LEDs and powering wrist watches. Further, the WR-SE-TENG device was used to scavenge bio-mechanical energy from human motions and also used for a real-time application of zero power consuming/self-powered pressure sensors. As an active sensor, the device showed linear sensing behavior and a sensitivity of 0.492 μA kPa^{-1}.

Received 19th December 2019
Accepted 20th December 2019

DOI: 10.1039/c9na00790c

rsc.li/nanoscale-advances

1. Introduction

Energy harvesting technologies have recently been the trending topic, which have potential as solutions to the global energy crisis. In recent years harvesting energy from sustainable energy sources such as wind,[1] water waves,[2,3] and bio-mechanical[4,5] and vibrational[6,7] sources has gained immense attention due to their simple energy conversion ability. Among them, energy harvesting from mechanical motions has expanded due to the abundant mechanical energy in daily life. Triboelectric nanogenerators (TENGs) are considered to be promising candidates for harvesting mechanical energy from various sources such as tides,[3] ocean waves,[8,9] human motions,[10] and strain.[11] Because of their simple design, cost-effective fabrication, highly reliable output performance and durability, many researchers are working towards their commercialization.[4] The first ever TENG was reported by Z. L. Wang's group in 2012 for harvesting mechanical energy[12] and utilized for small-scale energy harvesting. Currently, TENGs have been improved further with technological advancements, and used for energy harvesting and various applications in self-powered sensors.[13–15] In addition, many researchers are working to improve the output performance of TENGs by modifying the device structure, improving the surface contact area and doping.[16,17] In general, TENGs function *via* two major effects called triboelectrification and electrostatic induction. When two dissimilar triboelectric materials come into contact with each other either in vertical contact and separation or lateral sliding motion, a surface charge develops on the layers and drives the electrons to flow through an external load with the production of a potential drop.[18] This shows that the proper selection of active layers is the major paradigm in designing high performance TENG devices.

Next, to design the high performance TENG devices, two key factors needs to be considered: (i) surface charge

[a]*Nanomaterials and Systems Laboratory, Major of Mechatronics Engineering, Faculty of Applied Energy System, Jeju National University, Jeju, Republic of Korea. E-mail: kimsangj@jejunu.ac.kr; vivek@jejunu.ac.kr; alluri@jejunu.ac.kr; yuvasreep@jejunu.ac.kr; arunecebe@jejunu.ac.kr*

[b]*Nanosensors and Nanoenergy Lab, Department of Sensors and Biomedical Technology, School of Electronics Engineering, Vellore Institute of Technology, Vellore, India. E-mail: Arunkumar.c@vit.ac.in*

† Electronic supplementary information (ESI) available. See DOI: 10.1039/c9na00790c

generation increases with an increase in applied pressure and (ii) surface charge increases with an increase in contact points according to the Volta-Helmholtz hypothesis.[19] The most suitable route to multiply the contact point is to create surface roughness on the active layers. There are several techniques to create surface roughness such as photolithography, reactive ion etching, inductively coupled plasma etching, and thermal imprint lithography.[20–22] However, these techniques involve high cost, careful operation, and are time consuming.[23] Similarly, a major drawback of TENGs is their stability under moist and humid environmental conditions.[24] There is strong evidence proving that the output performance of TENGs is reduced drastically due to humidity, which hampers their full-fledged commercialization for daily use.[25–27] Recently, TENGs have been designed to humidity resistant by developing their active layers *via* super hydrophobic techniques.[28] However, still, the selection of materials, cost and time consuming processes make this a complicated process.

To overcome the above limitations, herein, we report a water-resistant silicone elastomer-based triboelectric nanogenerator (WR-SE-TENG), which is impervious in nature. The device was configured with a metal-dielectric configuration using nickel (Ni) foam and a micro roughness-created silicone elastomer film as the active triboelectric layers. The silicone elastomer film was fabricated *via* an easy and cost-effective soft lithography technique using commercial micro roughness sandpaper. Ni foam, which has a porous network structure, contributes to high surface roughness, and thus was used directly as the positive triboelectric layer. Ni foam having a porous nature could not damage the roughness on the silicone elastomer layer during the contact and separation process, making the output stable for a prolonged duration. The device was laminated using a polyethylene sheet with the help of a pouch laminator inside a glove box. The packing resists water and humidity, which affects the performance of the TENG. The output performances of the silicone elastomer (SE-TENG) device with different positive layers such as aluminum (Al), copper (Cu), and nickel (Ni) foam were also compared. Among them, SE-TENG made of Ni foam as the positive layer generated a maximum voltage and current of ~370 V/6.1 μA with a maximum area power density of ~17 mW m^{-2} at 1 GΩ load resistance. The stability of SE-TENG was analyzed for 2000 s and the stability of WR-SE-TENG was analyzed under various relative humidity ranging from 10% RH to 99% RH. This approach proves that the device was protected from humidity as well as stable in its output performance without a decrease in its efficiency. The device was used successfully for charging commercial capacitors, glowing light emitting diodes (LEDs) and powering up electronic wrist watches. Further, the WR-SE-TENG device was used for scavenging bio-mechanical energy from human motions such as finger tapping, palm tapping and foot tapping and LED glowing under bio-mechanical motions. The above experiments and tests prove that the WR-SE-TENG device is a promising sensor device to work under harsh and humid weather conditions.

2. Experimental

2.1 Fabrication of silicone elastomer film by soft lithography technique

The negative triboelectric material was made by replicating the micro rough pattern on sandpaper through the soft lithography technique. The dielectric layer was made by mixing an equal volume ratio of 1 : 1 (Ecoflex silicone 00-30) liquid silicone in a beaker followed by pouring it on to a piece of sandpaper. The liquid silicone poured sandpaper was then kept at 30 °C and allowed to cure for 6 h. After curing, the silicone film was peeled off slowly from the sandpaper to obtain the roughness-created silicone film.

2.2 Fabrication of water-resistant SE-TENG device

Next, to fabricate the TENG device, two PET films with the dimensions of 4 × 4 cm^2 were used as the supporting frames in the contact and separation device. Aluminum (Al) foils with an area of 3 × 3 cm^2 were attached on the bottom PET film through the center, followed by attaching the copper (Cu) wires using silver paste. Then, the silicone film was cut into the dimensions of 3 × 3 cm^2 and attached on the Al foil. To fabricate the positive layer, nickel (Ni) foam was selected and attached to the top PET sheet using double-sided tape and Cu electrodes were attached in a similar fashion. The air gap between both layers was fixed at 5 mm. Further, two other TENG devices were fabricated using Al and Cu as positive electrodes for the comparison and performance analysis of the TENG device. Further, the device was covered with polyethylene and sealed completely using a pouch laminator to make WP-TENG.

2.3 Characterization and electrical measurement

The surface morphology of the Ni foam and micro roughness silicone films were characterized using a field-emission scanning electron microscope (FE-SEM, TESCAN, MIRA 3). The electrical output analysis of voltage and current was performed using an electrometer (Keithley 6514 Instruments Inc., USA) and SR 570 low noise current amplifier (Stanford research Systems, USA), respectively. The external force for measuring the electrical output was applied using a linear motor (LinMot, Inc., Switzerland). A software platform using LabVIEW was built for real-time data acquisition and electrical analysis. A grounded home-made Faraday cage was set up for electrical measurements.

3. Results and discussion

Fig. 1a shows the layer-by-layer schematic of the SE-TENG device and its digital photographic image. The triboelectric layers are made of nickel foam and roughness-created PDMS film. The FE-SEM image shows the structure of the Ni foam and the micro roughness created *via* the soft lithography technique. Fig. 1b shows the step-by-step fabrication of the SE-TENG device. The device fabrication started with the preparation of supporting substrates for the contact and separation-based TENG, followed by placing electrodes on either sides. The

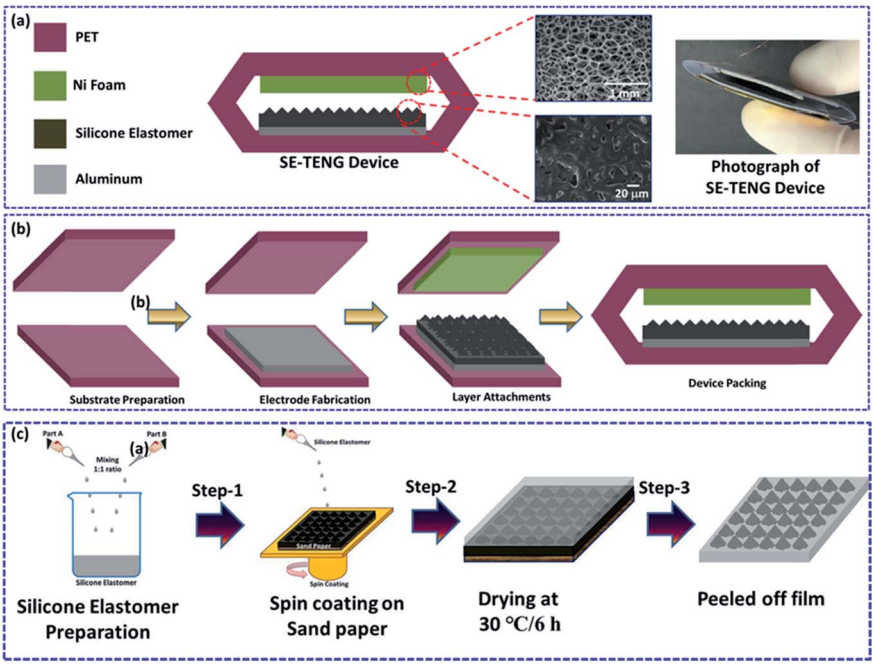

Fig. 1 SE-TENG device schematic and fabrication. (a) Layer-by-layer schematic of the SE-TENG device and the inset shows the FE-SEM morphology of the porous Ni foam and roughness-created silicone elastomer film with a photograph of the device. (b) Step by step schematic showing the SE-TENG device fabrication with every working layer used in the device. (c) Step-by-step fabrication of the silicone elastomer film from liquid silicone *via* the soft lithography technique using micro-roughness sandpaper.

electrodes themselves act as positive triboelectric layers, whereas the negative triboelectric layer was fabricated *via* a soft lithography technique. By using this technique the micro structured roughness was transferred to the silicone elastomer film from sandpaper. The detailed fabrication process is explained in the Experimental section. Fig. S1† shows the triboelectric series chart showing the triboelectric materials used in the fabrication of the SE-TENG device. Fig. 1c represents a schematic chart of the preparation of the silicone elastomer film *via* the cost effective soft lithography technique. Silicone elastomer part A and part B were mixed equally in a 1 : 1 ratio in a beaker. The solution was then poured dropwise on a piece of sandpaper and spread evenly through the spin coating technique. The silicone elastomer coated sandpaper was then dried at 30 °C for 6 h. After drying, the film was peeled off from the sandpaper and utilized as an active layer in the SE-TENG. The detailed film preparation process is explained in the experimental section. The working mechanism of SE-TENG is depicted in Fig. 2a–d, which is because of the triboelectric and electrostatic effects. In the initial condition, the top electrode is in contact with the bottom dielectric layer with no flow of electrons in the electrodes. Due to the mechanical motion applied on the device, the layers separate from each other, leading to the occurrence of a charge difference across the electrodes. This phenomenon induces the electrons to move from the top electrode to the bottom electrode through the external circuit. This action is responsible for the first half cycle of the electrical output signal (alternating current (AC)). With further actuating motion on the device, the layers again move close to each other, which induces the electrons to flow in the reverse direction, leading to the generation of a second half cycle. The potential distribution of the device was theoretically analyzed *via* a simple finite element simulation using the COMSOL Multiphysics software. Fig. 2e–g show the surface potential distribution from the contact state until the maximum release state.

The electrical output analysis was performed for the TENG devices made of Al, Cu and Ni foam as positive electrodes and silicone elastomer remained as the negative triboelectric layer. Fig. 3a–c show the electrical output comparison of the TENG devices made of Al, Cu and Ni foam positive electrodes. The output was higher in case of the TENG device made of Ni foam. As is known, the roughness in the triboelectric layers plays a major role in the enhancement of the electrical output. Similarly, Ni foam, which has a porous nature, has a good surface roughness as well as a positive triboelectric property, which proved to be a suitable material for contact electrification. On the other hand, the Al and Cu films do not have any surface roughness or porosity on their surface. The drawback with a plain positive side and a micro roughness negative layer is the damage of the roughness after few actuations. However, the Ni foam and roughness-created negative layer led to an enhancement in the contact area as well as the triboelectric charge generation. The porous layer in the positive side under contact and separation working mode did not damage the roughness present in the negative side, which made the output stable for a prolonged period. The maximum electrical output obtained from the SE-TENG with an Ni electrode was ~370 V/6.1 μA. In contrast, the SE-TENG made of Cu and Al as the positive layer generated a maximum electrical output of ~180 V/2.5 μA

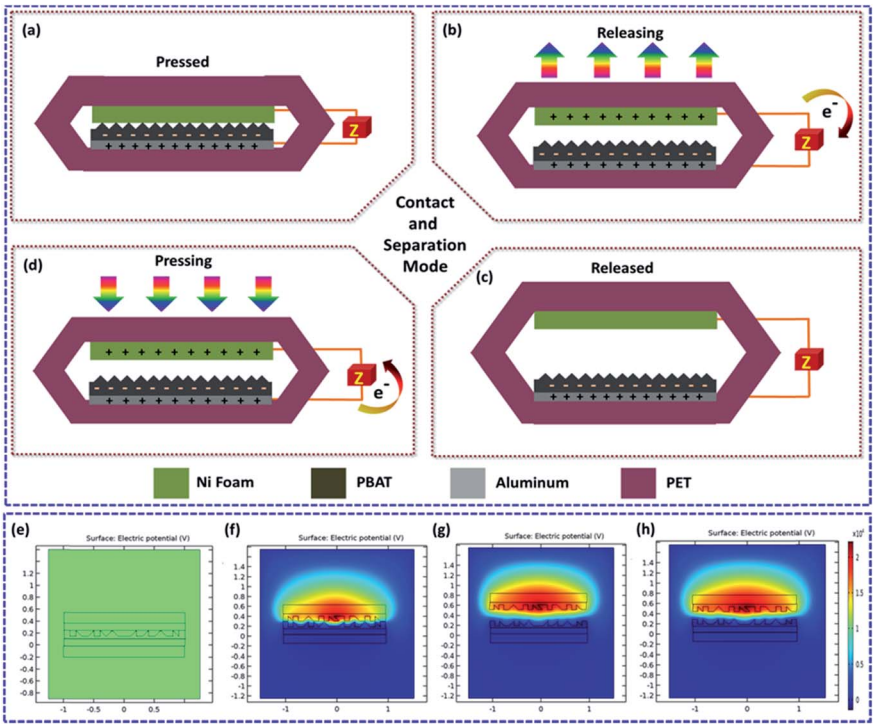

Fig. 2 Working mechanism of SE-TENG. (a–d) Contact and separation mode working mechanism of SE-TENG device with pressing and releasing motion and the respective electron flow directions. (e–h) Potential distribution of SE-TENG at various separation distances using the COMSOL software.

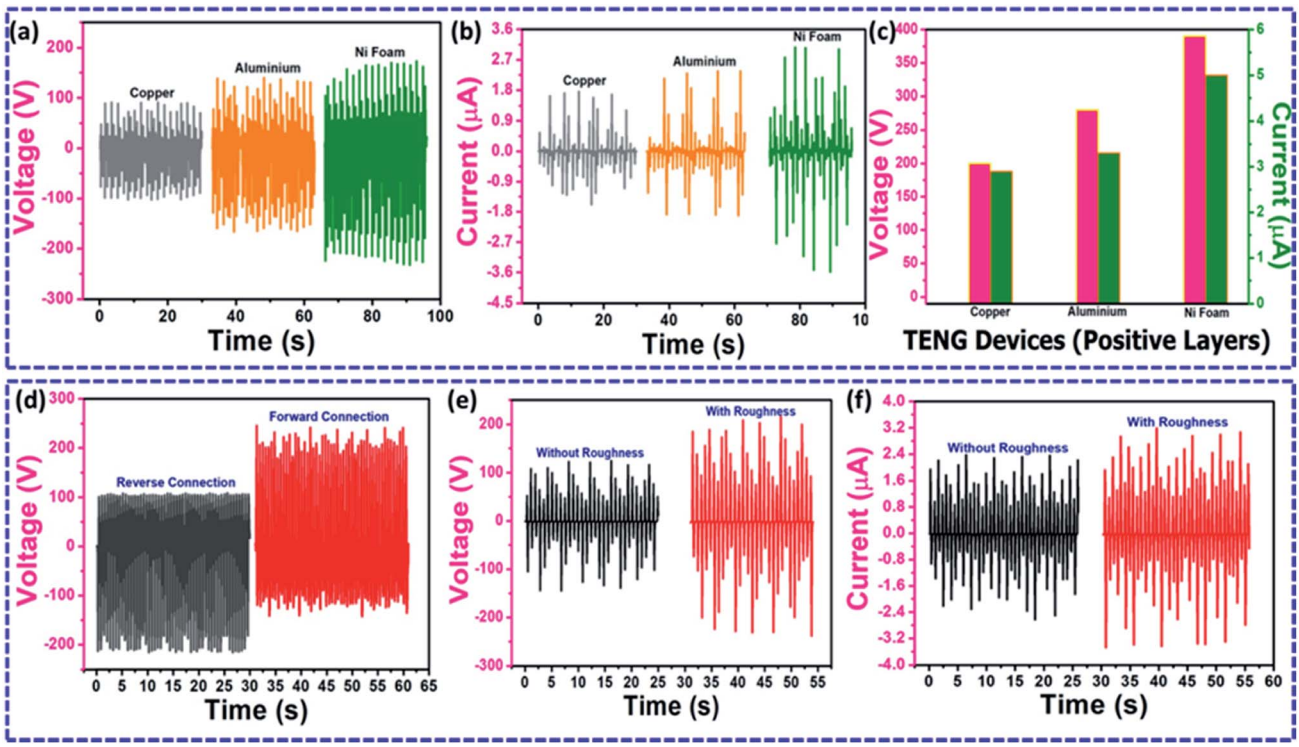

Fig. 3 Electrical output analysis of SE-TENG device. (a–c) Voltage and current output comparison of SE-TENG device showing the maximum electrical output with Ni foam as the positive triboelectric material. (d) Voltage signal showing the polarity test of SE-TENG with forward and reverse connection characteristics. (e and f) Electrical output performance comparison of silicone elastomer film with roughness and without surface roughness.

and ~270 V/3.6 μA, as shown in Fig. 3a and b, respectively. Fig. 3c shows the performance of the electrical output and the difference with respect to the positive layers. The silicone elastomer layer showed a maximum charge quantity of 160 nC. Further analysis and applications were performed using the Ni foam SE-TENG device due to its high electrical output performance. To confirm the electrical output, which is purely from the triboelectric effect, a switching polarity test was carried out by switching the polarity of the TENG device during its measurement. The device showed an exact 180° phase shift in its generated electrical output signal. This clearly confirms that the electrical output is purely from the SE-TENG device, as shown in Fig. 3d. To prove the contribution of surface roughness and its role in enhancing the electrical performance, the electrical measurement was carried out with two SE-TENG devices, one made of the roughness-created elastomer film and the other with a plain film. The electrical output clearly evidenced that the SE-TENG made of the surface roughness-created elastomer film showed a higher output than the plain elastomer film, as shown in Fig. 3e and f, respectively.

To validate the electrical output of the SE-TENG device, various confirmatory tests were performed, such as charging commercial capacitors, glowing LEDs, and powering up a digital wristwatch. Fig. 4a shows the charging characteristics of various rating commercial capacitors such as 0.22 μF, 1 μF, 10 μF and 22 μF for a period of 150 s. The inset in Fig. 4a shows the charging pattern during the device contact and separation with respect to external motion using a linear motor. Fig. S2† shows the circuit diagram, which was used for performing the capacitor charging. The capacitor with the lowest rating 0.22 μF charged quickly to 31 V in 150 s, storing a maximum energy of 99 μJ. Similarly, the capacitor with the highest rating stored a maximum energy of 11 μJ, which was charged to 0.9 V in 150 s. The other two capacitors, 1 μF and 10 μF, charged to 5 V and 2 V with the maximum energy storage of 125 μJ and 18.05 μJ, respectively as shown in Fig. 4b. Fig. 4c shows the charging and discharging cycle of a 10 μF commercial capacitor under the mechanical force of 10 N. The capacitor stored 5 V in 150 s and the force was removed. Consequently, this made the capacitor discharge the stored potential to 3.5 V. The cycle was repeated two more times to show the cyclic stability of the commercial capacitor charging and discharging. The SE-TENG device showed a maximum area power density of ~17 mW m^{-2} at 1 GΩ load resistance, as shown in Fig. 4d. This indicates that 1 GΩ resistance was the exact load-matching resistance for the SE-TENG device, which can be used further for focusing in the real-time applications. To show the durability of the SE-TENG device, a stability test was carried out for a period of 2000s, as shown in Fig. 4e and the stability pattern is shown in Fig. S5.† The inset shows the uniform peak pattern (every 600 s) from the start of the test until 2000 s. This shows that the device can work for a long period of time with a stable electrical output. Further,

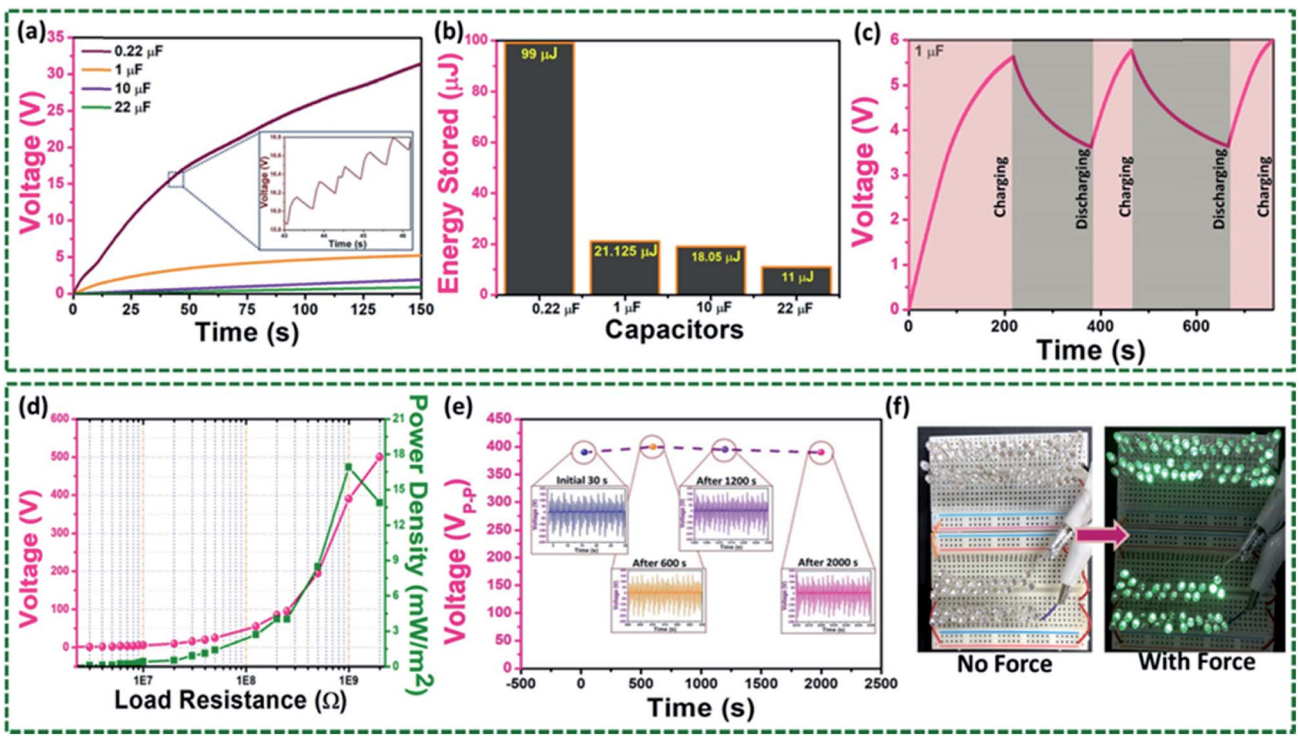

Fig. 4 Real-time output analysis and durability test for SE-TENG device. (a) Commercial capacitor charging characteristics with various capacitors such as 0.22 μF, 1 μF, 10 μF and 22 μF for a period of 150 s. (b) Energy storage analysis of the capacitors charged using the SE-TENG device. (c) Charging and discharging cyclic characteristics of 1 μF capacitor. (d) Impedance matching analysis and instantaneous area power density of SE-TENG device upon various resistance values; the device shows the maximum area power density of ~17 mW m^{-2} at 1 GΩ load resistance. (e) Stability analysis of SE-TENG showing its stable power delivering nature for a period of 2000 s. Inset shows the output peak pattern with the interval of 600 s. (f) 60 green LEDs glowing using SE-TENG upon applying force by pressing and releasing the device.

the SE-TENG was used to glow 60 green LEDs in series connection, as shown in Fig. 4f and Video S4.† These tests validate that the SE-TENG is a promising candidate for powering low power electronic devices.

Recently, one of the drawbacks faced by TENGs is their performance under the influence of humidity. The stability and performance of TENGs decrease due to a change in humidity. This is due to the interaction of moisture with the triboelectric layers, which leads to a reduction in surface charge generation. Thus, to overcome this issue, the SE-TENG was packed completely with a polyethylene pouch and sealed using a pouch laminator. The packing does not allow humidity, air or water droplets into the layers of the device. The water-resistance capability and the electrical response behavior of WR-SE-TENG is shown in Video S1.† A schematic and digital photograph of the water-resistant SE-TENG is shown in Fig. 5a. The water resistance capability of SE-TENG was tested by dipping the TENG device in a box full of water, as shown in Fig. S3.† The electrical output performance of the packed and unpacked SE-TENG is shown in Fig. 5b and c, respectively. The device shows a similar output performance with respect to packing in case of both voltage and current, proving that the performance was not reduced due to the packing. Fig. 5d and e show the electrical output of the water-resistant SE-TENG by finger pressing under water. The output showed the exact phase shift in signal after being packed and actuated inside the water tub. The inset in Fig. 5d shows the device immersed in water and the inset in Fig. 5e shows the LED glowing by pressing the device by placing it in water. Further, the water-resistant SE-TENG was tested under various relative humidity (% RH), as shown in Fig. 5f. The device worked stably in the humidity range of 10% RH to 99% RH. Fig. S3† shows the homemade humidity chamber used for performing the humidity test. This also confirms that the device was packed perfectly, and the influence of humidity does not affect the performance of the SE-TENG

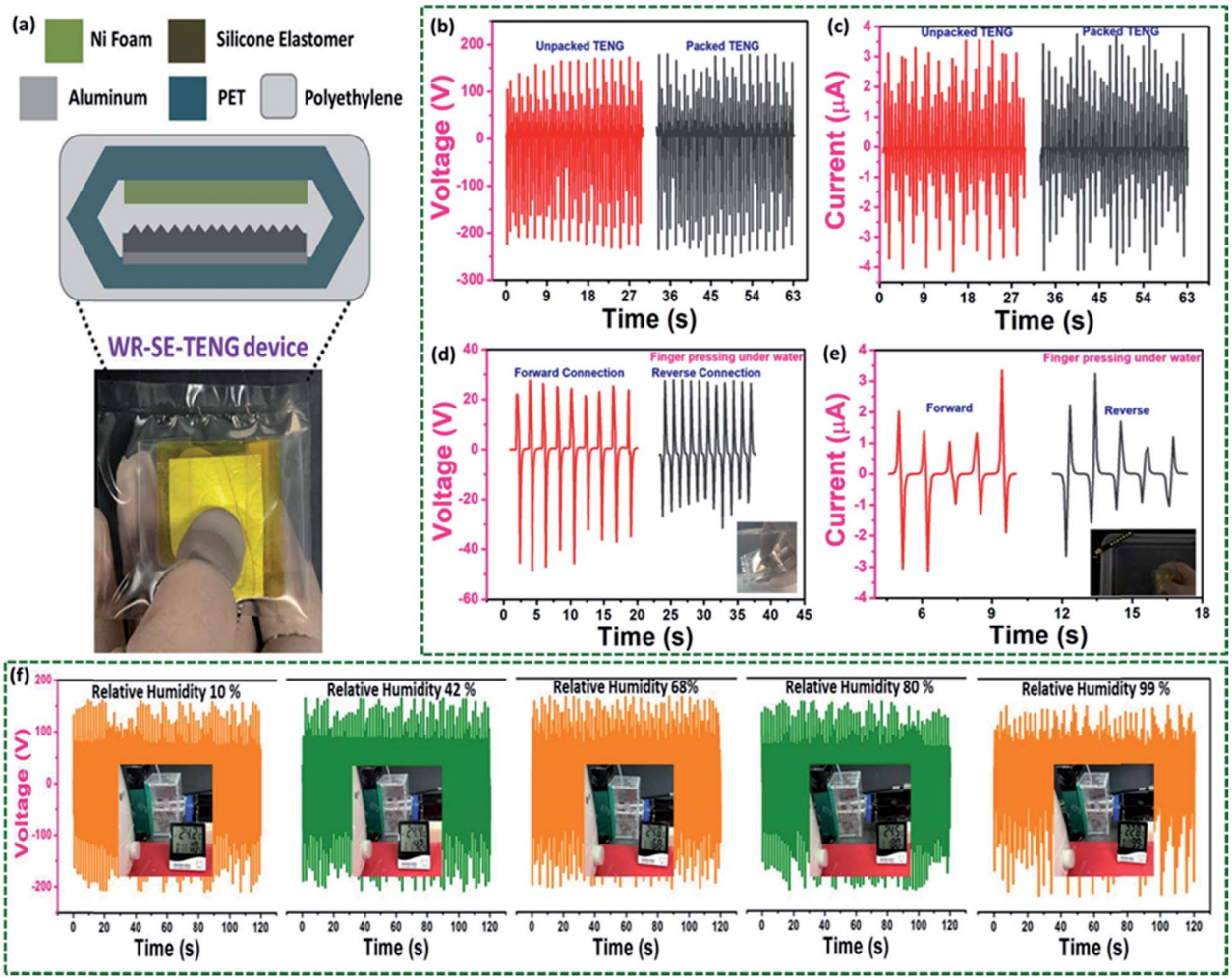

Fig. 5 Water-resistant SE-TENG device fabrication and its electrical performance. (a) Layer-by-layer schematic diagram of WR-SE-TENG device and digital photograph showing the device packed with polyethylene and placed inside water. (b and c) Voltage and current behavior of the packed and unpacked SE-TENG device, respectively. (d and e) Voltage and current behavior and polarity configurations of the WR-SE-TENG device when pressed inside a water tub, respectively. (f) Humidity test of the WR-SE-TENG device under various relative humidity of 10%, 42%, 68%, 80% and 99% RH, where the device showed a stable output for the entire period.

device. This proves that the packed TENG devices can be used in harsh weather and environmental conditions.

After undergoing various confirmatory tests and performance analysis experiments using the SE-TENG and water-resistant SE-TENG, the device was used for demonstrating a few real-time applications, which are mandatory for any type of energy harvester. Fig. 6a–f show the capability of SE-TENG for scavenging bio-mechanical energy from human hand and leg motions. The water-resistant SE-TENG device was attached on the floor using Scotch tape to avoid unwanted movements and

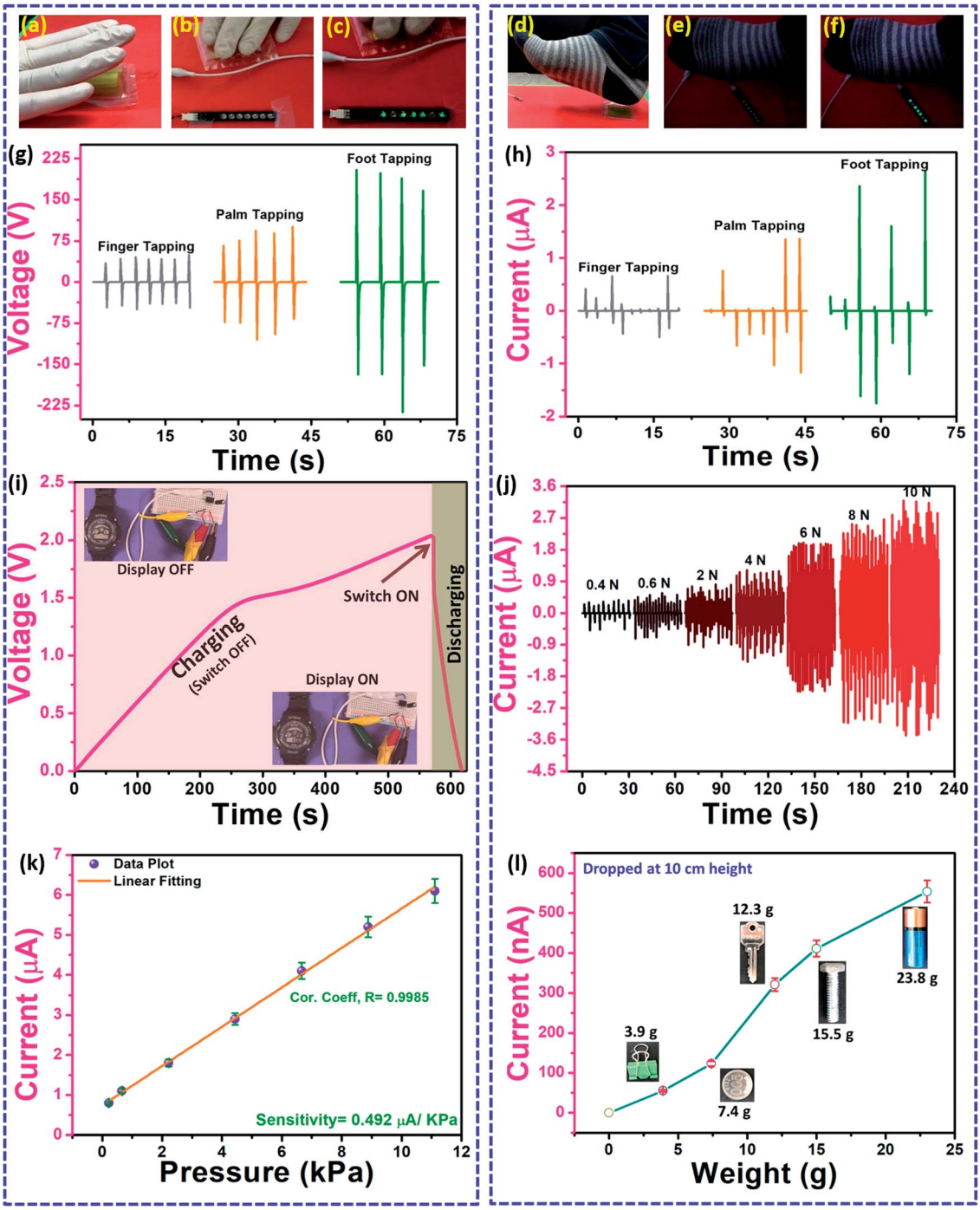

Fig. 6 Bio-mechanical energy harvesting and zero power consuming pressure sensor applications. (a–h) Digital photographs of the WR-SE-TENG device under hand and foot tapping motions and LED glowing under human motions. (i) Powering up an electronic wristwatch with the help of a 22 μF capacitor. (j) Force analysis of the WR-SE-TENG device upon various force from 0.4 N to 10 N and its current output profile. (k) Self-powered/zero power consuming pressure sensor with difference pressure level and the linear behavior of its current value showing a correlation coefficient of 0.9985 and good sensitivity of 0.492 μA kPa^{-1}. (l) Real-time response of different light-weight items (paper clip, coin, key, bolt and battery) dropped on the device and its corresponding electrical output response.

the LEDs glowed under human hand and leg motions. The biomechanical energy scavenging was demonstrated by analyzing the electrical signal by applying force by palm and leg tapping. This demonstration is shown in Videos S2 and S3.† The voltage and current were maximum during leg tapping, which is due to the weight and large pressure acting on the device, leading to the generation of a higher electrical output as shown in Fig. 6g and h. This demonstration gives clear evidence of utilizing SE-TENG as a bio-mechanical energy harvester to harness biomechanical motions in daily life. Similarly, a digital wristwatch was powered using the water-resistant SE-TENG using a commercial 22 μF capacitor, as shown in Fig. 6i. In addition to that the water resistant SE-TENG was demonstrated as a zero power consuming pressure sensor. The device was placed on a flat surface and different ranges of force applied initially and its current profile recorded. The current profile increased with an increase in the applied force, as shown in Fig. 6j. The sensing characteristics were studied based the relationship between the changes in pressure with respect to the increase in current. The sensor showed a linear response upon an increase in pressure with a sensitivity of 0.492 μA kPa^{-1} and the correlation coefficient of 0.9985, as shown in Fig. 6k. Fig. 6l shows the electric output response of the active pressure-sensing TENG device with its ability to detect the pressure of different weight objects falling from a height of 10 cm. This shows the ability of the device to detect pressure in low ratings. From the results and studies, it is clear that the water-resistant TENG can effectively be used as a self-powered force sensor in harsh and humid environments, such as in water tanks, water pipes and infusion pumps.

4. Conclusions

In summary, a highly reliable impervious SE-TENG was fabricated successfully using a roughness-created silicone elastomer and Ni foam as active layers. The cost-effective soft lithography technique was introduced for creating micro-roughness on the silicone elastomer film. With a similar configuration, two other TENG devices made of Al-SE and Cu-SE were fabricated and the electrical output was analyzed. Among the three devices, SE-TENG made of Ni foam showed a higher electrical output ~370 V/6.1 μA with a maximum area power density of ~17 mW m^{-2} at 1 GΩ load resistance. The device performance in real-time was demonstrated by charging commercial capacitors, glowing LEDs and powering a digital watch. The durability of the device was analyzed by performing a stability test for a period of 2000 s. To make the device to work actively in the harsh and humid environmental conditions, the device was fabricated as a water-resistant SE-TENG by packing it with polyethylene films and laminated tightly and demonstrated its water-resistant capability by actuating it inside a water tub. The electrical output comparison with respect to the packed and unpacked SE-TENG device was analyzed and performed a humidity test of actuating the device under various relative humidity (10% RH to 99% RH). The test showed that the performance of the TENG device was not affected due to humidity as well as the packing gives a stable protection to the SE-TENG device from humidity. Finally, the device was used to harness the bio mechanical energy from daily human motions such as finger, hand and foot tapping. Also, the device was demonstrated for the potential real-time application of a self-powered/zero power consuming pressure sensor, showing a good sensitivity of 0.492 μA kPa^{-1} and the correlation coefficient of 0.9985. The above experiments and demonstrations prove that SE-TENG is a promising candidate to be used for measuring variable pressures in harsh environments such as fluid pressure, gas pressure and water level indications.

Conflicts of interest

The authors declare no competing of financial interest.

Acknowledgements

This work was supported by the Basic Science Research Program through the National Research Foundation of Korea (NRF) grant funded by the Korean government (MSIT) (2018R1A4A1025998, 2019R1A2C3009747).

References

1 L. Zhang, B. Zhang, J. Chen, L. Jin, W. Deng, J. Tang, H. Zhang, H. Pan, M. Zhu, W. Yang and Z. L. Wang, Lawn Structured Triboelectric Nanogenerators for Scavenging Sweeping Wind Energy on Rooftops, *Adv. Mater.*, 2016, **28**(8), 1650–1656.
2 R. Lei, H. Zhai, J. Nie, W. Zhong, Y. Bai, X. Liang, L. Xu, T. Jiang, X. Chen and Z. L. Wang, Butterfly-Inspired Triboelectric Nanogenerators with Spring-Assisted Linkage Structure for Water Wave Energy Harvesting, *Adv. Mater. Technol.*, 2019, **4**(3), 1800514.
3 Y.-C. Lai, Y.-C. Hsiao, H.-M. Wu and Z. L. Wang, Waterproof Fabric-Based Multifunctional Triboelectric Nanogenerator for Universally Harvesting Energy from Raindrops, Wind, and Human Motions and as Self-Powered Sensors, *Adv. Sci.*, 2019, **6**(5), 1801883.
4 A. Chandrasekhar, N. R. Alluri, V. Vivekananthan, J. H. Park and S.-J. Kim, Sustainable Biomechanical Energy Scavenger toward Self-Reliant Kids' Interactive Battery-Free Smart Puzzle, *ACS Sustainable Chem. Eng.*, 2017, **5**(8), 7310–7316.
5 X. Chen, L. Miao, H. Guo, H. Chen, Y. Song, Z. Su and H. Zhang, Waterproof and stretchable triboelectric nanogenerator for biomechanical energy harvesting and self-powered sensing, *Appl. Phys. Lett.*, 2018, **112**(20), 203902.
6 M.-L. Seol, S.-B. Jeon, J.-W. Han and Y.-K. Choi, Ferrofluid-based triboelectric-electromagnetic hybrid generator for sensitive and sustainable vibration energy harvesting, *Nano Energy*, 2017, **31**, 233–238.
7 J. Chen, G. Zhu, W. Yang, Q. Jing, P. Bai, Y. Yang, T.-C. Hou and Z. L. Wang, Harmonic-Resonator-Based Triboelectric Nanogenerator as a Sustainable Power Source and a Self-Powered Active Vibration Sensor, *Adv. Mater.*, 2013, **25**(42), 6094–6099.

8 G. Liu, H. Guo, S. Xu, C. Hu and Z. L. Wang, Oblate Spheroidal Triboelectric Nanogenerator for All-Weather Blue Energy Harvesting, *Adv. Energy Mater.*, 2019, 1900801.

9 H. Wang, Q. Zhu, Z. Ding, Z. Li, H. Zheng, J. Fu, C. Diao, X. Zhang, J. Tian and Y. Zi, A fully-packaged ship-shaped hybrid nanogenerator for blue energy harvesting toward seawater self-desalination and self-powered positioning, *Nano Energy*, 2019, **57**, 616–624.

10 V. Vivekananthan, A. Chandrasekhar, N. R. Alluri, Y. Purusothaman, W. Joong Kim, C.-N. Kang and S.-J. Kim, A flexible piezoelectric composite nanogenerator based on doping enhanced lead-free nanoparticles, *Mater. Lett.*, 2019, **249**, 73–76.

11 Y. Purusothaman, N. R. Alluri, A. Chandrasekhar, V. Vivekananthan and S. J. Kim, Regulation of Charge Carrier Dynamics in ZnO Microarchitecture-Based UV/Visible Photodetector via Photonic-Strain Induced Effects, *Small*, 2018, **14**(11), 1703044.

12 F.-R. Fan, Z.-Q. Tian and Z. Lin Wang, Flexible triboelectric generator, *Nano Energy*, 2012, **1**(2), 328–334.

13 F.-R. Fan, L. Lin, G. Zhu, W. Wu, R. Zhang and Z. L. Wang, Transparent Triboelectric Nanogenerators and Self-Powered Pressure Sensors Based on Micropatterned Plastic Films, *Nano Lett.*, 2012, **12**(6), 3109–3114.

14 V. Vivekananthan, N. R. Alluri, Y. Purusothaman, A. Chandrasekhar, S. Selvarajan and S.-J. Kim, Biocompatible Collagen Nanofibrils: An Approach for Sustainable Energy Harvesting and Battery-Free Humidity Sensor Applications, *ACS Appl. Mater. Interfaces*, 2018, **10**(22), 18650–18656.

15 H. Guo, J. Chen, L. Tian, Q. Leng, Y. Xi and C. Hu, Airflow-Induced Triboelectric Nanogenerator as a Self-Powered Sensor for Detecting Humidity and Airflow Rate, *ACS Appl. Mater. Interfaces*, 2014, **6**(19), 17184–17189.

16 W. Liu, Z. Wang, G. Wang, G. Liu, J. Chen, X. Pu, Y. Xi, X. Wang, H. Guo, C. Hu and Z. L. Wang, Integrated charge excitation triboelectric nanogenerator, *Nat. Commun.*, 2019, **10**(1), 1426.

17 Q. Tang, M.-H. Yeh, G. Liu, S. Li, J. Chen, Y. Bai, L. Feng, M. Lai, K.-C. Ho, H. Guo and C. Hu, Whirligig-inspired triboelectric nanogenerator with ultrahigh specific output as reliable portable instant power supply for personal health monitoring devices, *Nano Energy*, 2018, **47**, 74–80.

18 T.-H. Chang, Y.-W. Peng, C.-H. Chen, T.-W. Chang, J.-M. Wu, J.-C. Hwang, J.-Y. Gan and Z.-H. Lin, Protein-based contact electrification and its uses for mechanical energy harvesting and humidity detecting, *Nano Energy*, 2016, **21**, 238–246.

19 W. R. Harper, *Contact and frictional electrification*, Laplacian Press: Morgan Hill, Calif., 1998.

20 X.-S. Zhang, M.-D. Han, R.-X. Wang, F.-Y. Zhu, Z.-H. Li, W. Wang and H.-X. Zhang, Frequency-Multiplication High-Output Triboelectric Nanogenerator for Sustainably Powering Biomedical Microsystems, *Nano Lett.*, 2013, **13**(3), 1168–1172.

21 X.-S. Zhang, M.-D. Han, R.-X. Wang, B. Meng, F.-Y. Zhu, X.-M. Sun, W. Hu, W. Wang, Z.-H. Li and H.-X. Zhang, High-performance triboelectric nanogenerator with enhanced energy density based on single-step fluorocarbon plasma treatment, *Nano Energy*, 2014, **4**, 123–131.

22 Y. Zhu, B. Yang, J. Liu, X. Wang, L. Wang, X. Chen and C. Yang, A flexible and biocompatible triboelectric nanogenerator with tunable internal resistance for powering wearable devices, *Sci. Rep.*, 2016, **6**, 22233.

23 B. Dudem, N. D. Huynh, W. Kim, D. H. Kim, H. J. Hwang, D. Choi and J. S. Yu, Nanopillar-array architectured PDMS-based triboelectric nanogenerator integrated with a windmill model for effective wind energy harvesting, *Nano Energy*, 2017, **42**, 269–281.

24 G. Zhu, Z.-H. Lin, Q. Jing, P. Bai, C. Pan, Y. Yang, Y. Zhou and Z. L. Wang, Toward Large-Scale Energy Harvesting by a Nanoparticle-Enhanced Triboelectric Nanogenerator, *Nano Lett.*, 2013, **13**(2), 847–853.

25 V. Nguyen and R. Yang, Effect of humidity and pressure on the triboelectric nanogenerator, *Nano Energy*, 2013, **2**(5), 604–608.

26 A. Chandrasekhar, V. Vivekananthan, G. Khandelwal and S. J. Kim, A fully packed water-proof, humidity resistant triboelectric nanogenerator for transmitting Morse code, *Nano Energy*, 2019, **60**, 850–856.

27 A. Chandrasekhar, G. Khandelwal, N. R. Alluri, V. Vivekananthan and S.-J. Kim, Battery-Free Electronic Smart Toys: A Step toward the Commercialization of Sustainable Triboelectric Nanogenerators, *ACS Sustainable Chem. Eng.*, 2018, **6**(5), 6110–6116.

28 K. Zhao, Z. L. Wang and Y. Yang, Self-Powered Wireless Smart Sensor Node Enabled by an Ultrastable, Highly Efficient, and Superhydrophobic-Surface-Based Triboelectric Nanogenerator, *ACS Nano*, 2016, **10**(9), 9044–9052.

